We are IntechOpen,
the world's leading publisher of
Open Access books
Built by scientists, for scientists

6,900
Open access books available

185,000
International authors and editors

200M
Downloads

154
Countries delivered to

Our authors are among the

TOP 1%
most cited scientists

12.2%
Contributors from top 500 universities

CLARIVATE ANALYTICS
BOOK CITATION INDEX
INDEXED

WEB OF SCIENCE™

Selection of our books indexed in the Book Citation Index
in Web of Science™ Core Collection (BKCI)

Interested in publishing with us?
Contact book.department@intechopen.com

Numbers displayed above are based on latest data collected.
For more information visit www.intechopen.com

Hydraulic Fracture Propagation Across a Weak Discontinuity Controlled by Fluid Injection

Dimitry Chuprakov, Olga Melchaeva and Romain Prioul

Additional information is available at the end of the chapter

Abstract

We investigated the problem of a hydraulic fracture propagation through a weakly cohesive frictional discontinuity for different conditions of fracture toughness, in situ stresses, fracture intersection angle, injection parameters and permeability of the pre-existing fracture. The parametric sensitivity of the fracture interaction process, in terms of crossing versus arresting of the hydraulic fracture at the discontinuity, was performed using numerical simulations through an extensive parameter space representative of hydraulic fracturing field conditions. The effect of the pre-existing fracture permeability on the crossing behavior was analyzed using a simple analytical model. We showed that the injection rate and viscosity of fracturing fluid are the key parameters controlling the crossing/non-crossing interaction behavior, in addition to already known fracture interaction angle and in-situ stress parameters. We have also found that the pre-existing fracture hydraulic aperture, when as large as that of the hydraulic fracture aperture, has significant influence on the interaction and may more likely cause the hydraulic fracture to arrest.

1. Introduction

The main function of a hydraulic fracture (HF) treatment is to effectively increase reservoir permeability and drainage by creating one or more conductive fractures that connect to the wellbore [1-2]. The stimulation treatments are especially necessary in low-permeability unconventional source rocks such as shales, which are not economical without fracturing [3] and sometimes even subsequent refracturing [4]. The modeling of HF propagation is important

to the design of the treatment and the ability to evaluate post-treatment production. Most fracture propagation models assume an oversimplified single planar geometry of fracture propagation [1, 5]. However, in highly heterogeneous and naturally fractured formations, the geometry of HFs can be complex because of their interaction with preexisting discontinuities in the rock, such as natural fractures, faults, and bedding interfaces [3, 6-7], which will be referred as NFs. For example, it is well known that an HF can be arrested by an NF or can reinitiate after the contact [8-16]. The result of the interaction depends on the in-situ stresses [10, 15, 17-18]; friction [12], cohesion [19], and permeable properties of the NF [20]; the rheological properties of the injecting fluid; and injection flow rate [21-22].

To predict the ultimate geometry of HFs, one needs to predict the result of every HF-NF interaction [23]. Several theoretical, numerical, and experimental studies have focused on this task [8, 10, 24-26]. One of the simplest analytical criterion for predicting the outcome of the HF-NF orthogonal interaction was developed by Renshaw and Pollard [18] and extended to arbitrary angle of interaction by Gu et al. [15]. This criterion predicts initiation of the secondary fracture (SF) on the opposite side of the interface influenced only by the friction, cohesion, and in-situ stresses. However, the HF activation and stress field near the intersection point are strongly dependent on the opening of the HF at contact and hence on pumping rate and fluid viscosity — a key point that has been ignored up to now [27]. Recent theoretical developments and laboratory experiments [21-22] have shown it is possible to derive an analytical crossing model taking into account the effect of flow rate and fluid viscosity on the HF-NF crossing behavior [27]. The results of this new HF-NF crossing model in a fracturing simulator environment are presented in a companion paper [28].

This paper offers dimensionless formulation and interpretation of the problem of fracture interaction. The numerical investigations are made by means of the code MineHF2D developed by Zhang et al. [20, 29]. This work focuses primarily on the parametric sensitivity analysis of the problem in terms of HF reinitiation at the NF and takes into account a more rigorous initiation criterion based on stress and energy premises.

The content of the paper is organized as follows. First, we define the problem of the HF-NF interaction mathematically and select all independent dimensionless parameters that influence the result. Next, we discuss the results of the parametrical study in terms of crossing or arresting behavior in the selected parametric diagrams. Finally, we concentrate on the particular effect of the hydraulic permeability of the NF by means of analytical and numerical models.

2. Problem statement

Consider the interaction between an HF and a preexisting discontinuity that represents a mechanically closed fracture with finite permeability, which is higher than that of the surrounding rock. In what follows the discontinuity will be referred to as an NF.

In nature, both the HF and the NF have certain 3D extents in the vertical and horizontal directions and their interaction should be described in 3D. If the vertical heights of the

fractures (perpendicular to the plane of Fig. 1) are far more comparable to or significantly exceed the horizontal size of the fractures affected by the interaction (in a plane of Fig. 1), the consideration of fractures can be reduced to plain-strain geometry. In this work we use a plain-strain model for the interacting fractures in the cross-sectional plane defined by the 1D flow direction (Fig. 1).
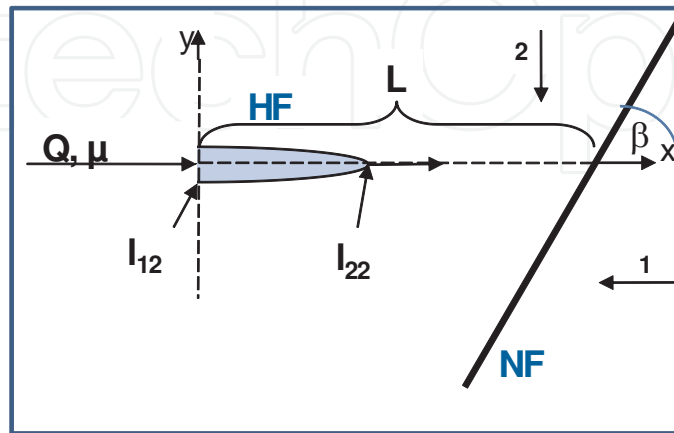

Figure 1. Schematic representation of the problem statement where a plain-strain (Khristianovich-Zheltov-DeClerk) model is considered with a one-wing HF is propagating toward a discontinuity (NF)

Suppose that the HF propagates from the injection point (point l_{11}= (0;0) in Fig. 1) toward the NF perpendicular to the minimum horizontal far-field stress σ_2, coinciding with axis Oy. When the HF reaches the NF (point l_{12}=(L;0) in Fig. 1) it forms a T-shape contact with an angle β. Maximum and minimum far-field stresses, σ_1 and σ_2, acting parallel to x- and y-axes respectively, are constant and uniformly distributed. The rock is assumed impermeable, isotropic, and elastic.

Following Zhang and Jeffrey [12], the elasticity equations for the system of interacting fractures can be written as the following sum of the contributions from each fracture with coordinates of their tips l_{i1}, l_{i2}, where i = 1,2, (1 refers to the HF, 2 refers to the NF):

$$\begin{cases} \sigma_n(x, y) - \sigma_n^\infty(x, y) = \sum_{i=1}^{N} \frac{E}{2\pi(1 - \nu^2)} \int_{l_{i1}}^{l_{i2}} [G_{11}(x, y, \xi)w(\xi) + G_{12}(x, y, \xi)v(\xi)]d\xi \\ \tau(x, y) - \tau^\infty(x, y) = \sum_{i=1}^{N} \frac{E}{2\pi(1 - \nu^2)} \int_{l_{i1}}^{l_{i2}} [G_{21}(x, y, \xi)w(\xi) + G_{22}(x, y, \xi)v(\xi)]d\xi \end{cases} \tag{1}$$

where integration is performed along the fracture path, N is the number of fractures (initially N = 2), G_{ij} is the hypersingular Green's functions for this problem [30-32], E is Young's modulus, ν is Poisson's ratio. The equations describe the integral relationship between the net normal and shear stress applied at the fracture, σ_n and τ respectively, and fracture opening and sliding, w and v respectively. Frictional slippage at the NF obeys the following Mohr-Coulomb friction criterion with cohesion C and friction coefficient λ:

$$|\tau| = \lambda(\sigma_n - p_f) + C \tag{2}$$

where p_f is the fluid pressure in the NF. The mechanically closed NF can possess a finite hydraulic permeability, which is significantly higher than that of the surrounding rock. To describe the NF permeability the concept of hydraulic aperture w_h is introduced. Hydraulic aperture is an imaginary opening of the closed crack simulating the residual conductivity of the NF and does not contribute to stress change. The permeability of the NF, k, and the hydraulic opening, w_h, are related by

$$k = \frac{w_h^2}{12} \tag{3}$$

If the fluid penetrates the closed NF, the hydraulic aperture w_h can be changed depending on the infiltrated fluid pressure in the NF. When the fluid pressure exceeds the normal stress applied to the NF, the NF will open mechanically, leading to the associated increase of its hydraulic aperture, which is the sum of mechanical and hydraulic opening, and

$$k = \frac{\left(w + w_h\right)^2}{12} \tag{4}$$

To describe the dependency of the hydraulic aperture w_h on the fluid pressure p_f, a nonlinear spring model is used [20]:

$$\frac{dw_h}{dp_f} = \chi w_h \tag{5}$$

where χ is the empirical constant of order of 10^{-8}Pa^{-1} - 10^{-6}Pa^{-1} that characterizes the compliance of a NF with respect to the increase of net pressure inside the fracture.

Restricting our study to incompressible and Newtonian fluids, the fluid flow in the growing HF is described by the following continuity equation and Poiseulle's law:

$$\frac{dw}{dt} + \frac{dq}{dx} = 0 \tag{6}$$

$$q = -\frac{w^3}{12\mu}\frac{dp_f}{dx} \tag{7}$$

where q is the 1D flow rate inside the fracture, and μ is the dynamic fluid viscosity. For fluid flow inside the NF, the same equations can be written with slight modification of the total hydraulic opening, so that

$$\frac{d(w + w_h)}{dt} + \frac{dq}{dx} = 0 \tag{8}$$

$$q = -\frac{(w + w_h)^3}{12\mu} \frac{dp_f}{dx} \tag{9}$$

At the inlet of the HF the fluid flow is prescribed as constant:

$$q(x = 0, t) = Q_0 \tag{10}$$

When the HF and the NF are in contact at the junction point, the fluid flux is required to satisfy the local continuity equations, meaning that the income flux from the HF is equal to the flux outgoing to the NF. Additionally, the fluid pressure profile along the HF and the NF must have a common value at the junction point. The coupling condition at the junction is

$$
\begin{aligned}
p_f^{(HF)}(x = L) &= p_f^{(NF)}(x' = 0) \\
q(x = L) &= q(x' = +0) + q(x' = -0)
\end{aligned}
\tag{11}
$$

The imposed boundary conditions at the inlet and junction point are sketched in Fig. 2.
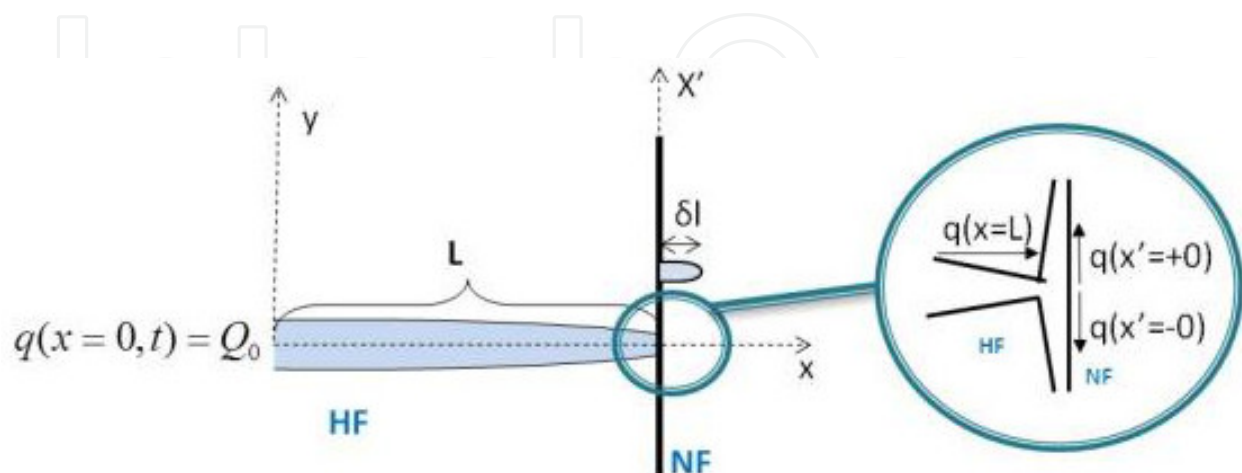

Figure 2. Boundary conditions of the problem

The condition for the HF tip propagation implies the quasi-static growth of the Mode I fracture such that Mode I stress intensity factor at the tip of the HF, K_I, equals the fracture toughness of rock K_{IC}:

$$K_I = \frac{w(x)E}{4(1-\nu^2)}\sqrt{\frac{\pi}{2}}\frac{1}{\sqrt{l_{(op)} - x}}\bigg|_{l_{(op)}-x \ll l_{(op)}} = K_{IC} \tag{12}$$

where $l_{(op)}$ is the half-length of the open fracture zone. A condition similar to zero toughness can be written for the tip of the open zone created at the NF when the sliding zone propagates farther than the open zone. At the tip of the NF sliding zone we have then

$$K_{II}^{(NF)} = \frac{v(x)E}{4(1-\nu^2)}\sqrt{\frac{\pi}{2}}\frac{1}{\sqrt{l_{(sl)} - x}}\bigg|_{l_{(sl)}-x \ll l_{(sl)}} \leq K_{IIC}^{(NF)} \tag{13}$$

where $l_{(sl)}$ is the half-length of the sliding fracture zone. If the sliding zone and open zone coincide at cohesive NF, the following mixed mode criterion is used instead of (13):

$$\begin{cases} K_I^{(NF)} = K_{IC}^{(NF)} \\ K_{II}^{(NF)} = K_{IIC}^{(NF)} \end{cases} \tag{14}$$

Modeling of the new fracture initiation has been traditionally based on stress criterion only [26]. Following Leguillon [33], this work presents an extension in which the initiation of a new fracture must meet the joint stress and energy criteria, which is dependent on the initial length of the fracture initiated, δl. To create a new tensile crack, the stress acting normally to the crack must exceed tensile strength of the rock, T_0. Energy criterion for crack creation is simplified here to the requirement that the stress intensity factor at the initiated crack tip, K_I, exceeds fracture toughness of the rock, K_{IC}. Using the sign convention for the tensile stress to be negative, the joint initiation criterion used reads

$$\begin{cases} \sigma_{\tau\tau}(\delta l) \leq -T_0 \\ K_I(\delta l) > K_{IC} \end{cases} \tag{15}$$

where $\sigma_{\tau\tau}$ is the tangential normal stress parallel to the NF and evaluated along the initiated crack path. Once the new crack is initiated, its further growth is determined by the following criterion of mixed-mode fracture propagation [34]

$$\left[K_I \cos^2\frac{\theta}{2} - \frac{3}{2}K_{II}\sin\theta \right]\cos\frac{\theta}{2} = K_{IC} \tag{16}$$

where θ is the deflection angle from the original fracture tip growth orientation.

In what follows we are interested in the ultimate result of the HF-NF interaction. After the contact with the NF, the HF can either stay arrested by the NF or reinitiate at the NF and continue propagation to the remainder of the rock behind the NF. Possible outcomes of HF-NF interaction are schematically drawn in Fig. 3.

In the case of arresting, the NF is extensively activated in opening and sliding such that the tensile stresses near the HF tip become insufficient for continuous fracture propagation or initiation of a new crack behind the NF. After the contact, the fracturing fluid is injected into the NF and the dilated NF becomes a part of a complex hydraulic fracture network. In contrast, if the NF appears to be frictionally or cohesively strong, the HF will reinitiate at the NF and continue its propagation into the remainder of the rock. The fracture often reinitiates at the offset positions, forming a more complex kinked fracture path after the interaction with the NF.

In this work, the problem of the HF-NF interaction is solved by means of the computational code developed by Australia's Commonwealth Scientific and Industrial Research Organization, CSIRO. The details of numerical scheme implemented in this code can be found in [12-13, 20, 24, 29].
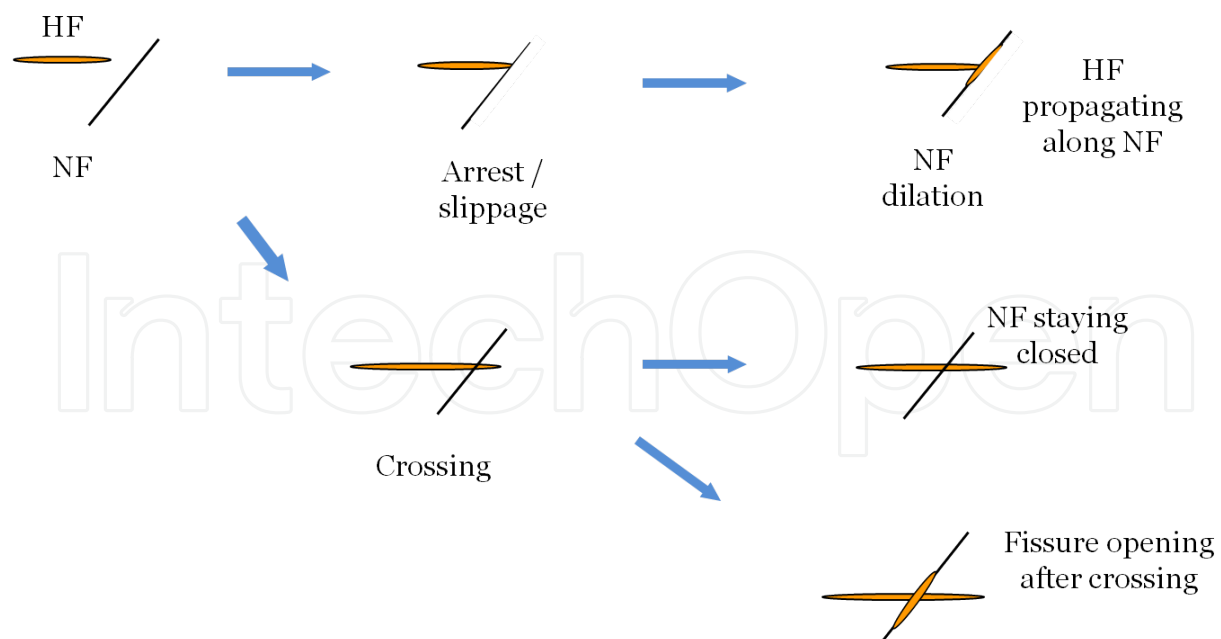

Figure 3. Schematic diagram of possible HF-NF interaction scenarios

3. Parameterization of HF-NF problem

The complete system of coupled equations (1, 5-7) subject to the boundary and initial conditions (2, 10-14) and criteria for crack initiation and propagation (15-16) is a complex multiparameterized problem. The aim of the work is to study parametric sensitivity of the result of HF-NF interaction, and the challenge of this undertaking substantially grows with the number of the independent parameters in the study. Our first initiative is to come up with proper parameterization of the problem that will be used in the numerical computations.

There are 14 dimensional parameters that impact the solution: injection rate into fracture, Q_0; fracturing fluid viscosity, μ; plain-strain Young's modulus, $E' = E/(1 − v^2)$; Mode I fracture toughness of the rock, K_{IC}; tensile strength of the rock, T_0; maximum in-situ stress, σ_1; minimum in-situ stress, σ_2; length of the HF at contact with the NF, L; angle between the fractures, β; friction coefficient, λ; Mode I NF toughness, $K_{IC}^{(NF)}$ Mode II NF toughness, $K_{IIC}^{(NF)}$; hydraulic permeability of the NF, k, which is coupled to the residual NF opening as $k = w_h^2 / 12$; and NF compliance, χ. For the sake of concise expressions, we introduce the following notations for viscosity $\mu' = 12\mu$, for the fracture toughness in rock $K_{IC}^{'} = \sqrt{32/\pi} K_{IC}$, and at the NF $K_{IC}^{(NF)'} = \sqrt{32/\pi} K_{IC}^{(NF)}$, $K_{IIC}^{(NF)'} = \sqrt{32/\pi} K_{IIC}^{(NF)}$.

Table 1 summarizes the expected range of dimensional parameters for the majority of HF jobs in unconventional reservoirs from various sources [35-36]. The data were obtained from laboratory experiments and field measurements.

	Parameter	Range
Q	Volumetric injection rate	0.01–0.25 m³/s mmoposdvrgenmk m³/sec
L	Distance between HF and NF	1–10 m
μ	Fluid viscosity	1–1000 cP
E	Young's modulus	9–110 GPa
v	Poisson's coefficient	0.11 –0.252
K_{IC}	Mode I fracture toughness	0.1–2.7 MPa(m$^{1/2}$)
$K_{IC}^{(NF)}/K_{IC}^{(HF)}$	Toughness ratio for NF vs. rock matrix	0–0.5
$K_{IIC}^{(NF)}/K_{IC}^{(NF)}$	Toughness ratio for NF	~1
σ_1	Maximum in-situ stress	13–105 MPa
σ_2	Minimum in-situ stress	11–100 MPa
λ	Friction coefficient at the NF	0.2–1
k_h	Permeability of NF	1 md–1 darcy
β	Fracture interaction angles	30˚–90˚

Table 1. Range of the problem's dimensional parameters specific to gas shale fracturing jobs

Let us normalize the equations by the convenient choice of the scaling. First we introduce the displacement scale W for the opening, shear displacement of the fractures, and the residual aperture of the NF as

$$w = \Omega W, \quad v = \Psi W, \quad w_h = \Omega_h W \tag{17}$$

where Ω, Ψ and Ω_h are the dimensionless opening, sliding, and residual NF opening, respectively. The fluid flow rate is scaled by the injection rate at the inlet $Q = Q_0$ as

$$q = \tilde{q} Q_0 \tag{18}$$

where $\tilde{q}$ is the dimensionless flow rate. Similarly, we introduce the dimensionless fluid pressure, Π, and stress components, Σ_i, with the stress and pressure scale P

$$p_f = \Pi P, \quad \sigma_n = \Sigma_n P, \quad \tau = \Sigma_\tau P, \quad \sigma_i = \Sigma_i P \tag{19}$$

The coordinates, including coordinates of fracture tips, are scaled by the length of the contacted fracture L as

$$(x, y) = (\bar{x}, \bar{y}) L, \quad l_{ij} = \gamma_{ij} L \tag{20}$$

and the time is scaled by a certain time scale T as

$$t = \bar{t} T \tag{21}$$

After substitution of (17-21) into equations (1-13) we obtain these seven dimensionless groups

$$\alpha_1 = \frac{TQ}{WL}, \quad \alpha_2 = \frac{W^3 P}{Q\mu' L}, \quad \alpha_3 = \frac{E'W}{PL}, \quad \alpha_4 = \frac{Q_0}{Q} = 1,$$

$$\kappa_{IC} = \frac{K'_{IC}\sqrt{L}}{WE'}, \quad \kappa_{IC}^{(NF)} = \frac{K_{IC}^{(NF)'}\sqrt{L}}{WE'}, \quad \kappa_{IIC}^{(NF)} = \frac{K_{IIC}^{(NF)'}\sqrt{L}}{WE'} \tag{22}$$

Choosing the viscosity scaling by setting $\alpha_i = 1$ in (22), we define the following expressions for the chosen scales:

$$W = \sqrt[4]{\frac{L^2 Q\mu'}{E'}}, \quad P = \sqrt[4]{\frac{E'^3 Q\mu'}{L^2}}, \quad T = \sqrt[4]{\frac{L^6 \mu'}{E' Q^3}} \tag{23}$$

After the scaling we obtain nine dimensionless parameters $\left(\kappa_{IC}, \kappa_{IC}^{(NF)}, \kappa_{IIC}^{(NF)}, \Sigma_1, \Sigma_2, \Omega_h, \beta, \lambda, \chi\right)$ that characterize our dimensionless problem. We also note the parameters have nonequal sensitivity to the result of fracture interaction. For example, all previous theoretical and experimental studies have shown that the significant effect of the relative difference of the applied stresses can be written as $\Delta\Sigma = (\Sigma_1 - \Sigma_2)/\Sigma_2$, rather than as the mean stress. The effect of NF compliance and the difference between Mode I and Mode II NF toughness can be neglected in the first attempt of parametric study, so we assume here $\kappa_{IC}^{(NF)} = \kappa_{IIC}^{(NF)}$. Consequently, we restrict our parametric analysis with the following six parameters $\left\{\kappa_{IC}, \Delta\Sigma, \beta, \lambda, \kappa_{IC}^{(NF)}, \Omega_h\right\}$.

This study is mainly intended for the oil and gas industry, so the comprehensive numerical study in infinite limits of these parameters in the present study is not necessary. In what follows we limit the range of the dimensionless parameter values to the practical range by use of the compilation of dimensional parameters of the problem shown in Table 1. Using the scaling introduced previously it is possible to calculate the corresponding range of the dimensionless parameters (Table 2).

Parameter	Minimum Value	Maximum Value
κ_{IC}	0.002	11
$\kappa_{IC}^{(NF)} / \kappa_{IC}^{(HF)}$	0	0.5
$\Delta\Sigma$	0	2
Ω_h	0.0001	0.37
β	30°	90°
λ	0.2	1

Table 2. Range of dimensionless parameters calculated from Table 1 using introduced scaling

The following parametric study is restricted to the range of values of dimensionless parameters shown in Table 2, as practically required.

4. Results of parametric study

We performed numerical simulations of the HF propagation and interaction with the preexisting NF by use of the modified CSIRO code (with stress-and-energy initiation criterion) [12, 20]. Dimensionless parameters of the simulations have been selected within the range specified in Table 2. Systematic analysis of the obtained results of HF-NF interaction allowed us to project them onto the specific parametric diagrams containing dimensionless toughness of the rock, fracture intersection angle, stress contrast, frictional coefficient. and relative toughness of the NF. For better representation they are divided into several cross sections of one global multiparametrical cube.

4.1. Dimensionless toughness κ_{IC} vs. angle β diagram

Fig. 4 shows the results of a large number of numerical computations performed with various independent parameters of the problem. They are projected on the diagram of dimensionless toughness versus interaction angle. These results represent the final outcome of the HF-NF interaction in terms of either fracture crossing or arresting at the NF. We observe that the HF crosses the NF predominantly at large angles of intersection (i.e., close to 90°) and smaller values of dimensionless toughness as expected. Note that the dimensionless toughness κ_{IC} we used for plotting depends not only on the Mode I toughness but also on the injection rate and fluid viscosity, as seen from Eqs. (22-23). If the fluid viscosity μ or the flow rate at the fracture inlet Q increases, the value of the dimensionless toughness decreases and the crossing behavior becomes more favorable.

The computations have been performed for several values of in-situ rock stress difference $\Delta\Sigma$. To denote this important parameter in the plotted results, we have used different colors for different values of $\Delta\Sigma$. To separate the crossing or arrest tendency at small stress contrast from the similar tendency at large stress contrast, we have presented the results (Fig. 4) in two diagrams for the small and large values of $\Delta\Sigma$ respectively. After using such a representation of the results, one can still observe that some points remained nonseparated and overlapped. For example, in the bottom diagram, the results from the computations with different stress contrast coincide at the same point in the angle-toughness diagram. They can have opposite outcome as shown by arrows at the bottom of Fig. 4.

4.2. κ_{IC} vs. $\Delta\Sigma$ diagram

The next series of parametric diagrams represent the results of numerical experiments in the dimensional toughness vs. stress contrast cross section. This representation better emphasizes the role of the dimensionless relative stress and with the flow rate and viscosity that are inversely proportional to the dimensionless toughness. Plots in Fig. 5 clearly show that the higher relative stress difference $\Delta\Sigma$, the larger the region of the dimensionless toughness values where fracture crossing occurs. The highest threshold value of the dimensionless toughness for crossing behavior increases with the stress contrast; i.e., in the formations with high stress contrast the crossing behavior will most probably happen even with low viscosity and/or low pumping rate during fracturing jobs. At the same time, it is unlikely that the rock with relatively small stress difference $\Delta\Sigma<1$ will support fracture crossing unless the dimensionless toughness value is sufficiently decreased by stronger injection power (larger pumping rates or higher fluid viscosity). This is especially the case if the preferential inclination of the NFs with respect to the orientation of the HF is far from 90°.

4.3. λ vs. $\kappa_{IC(NF)} / \kappa_{IC}$ diagram

Next we analyzed the influence of the friction coefficient λ and the relative NF Mode I toughness $\kappa_{IC(NF)} / \kappa_{IC}$ on the result of HF-NF interaction (Fig. 6). In this series of numerical tests we observe a sharp boundary for the friction coefficient values where the crossing behavior

ceases. We also observed that there is no influence of the relative NF toughness, compared to that of the friction, although this parameter deserves more attention in the future.
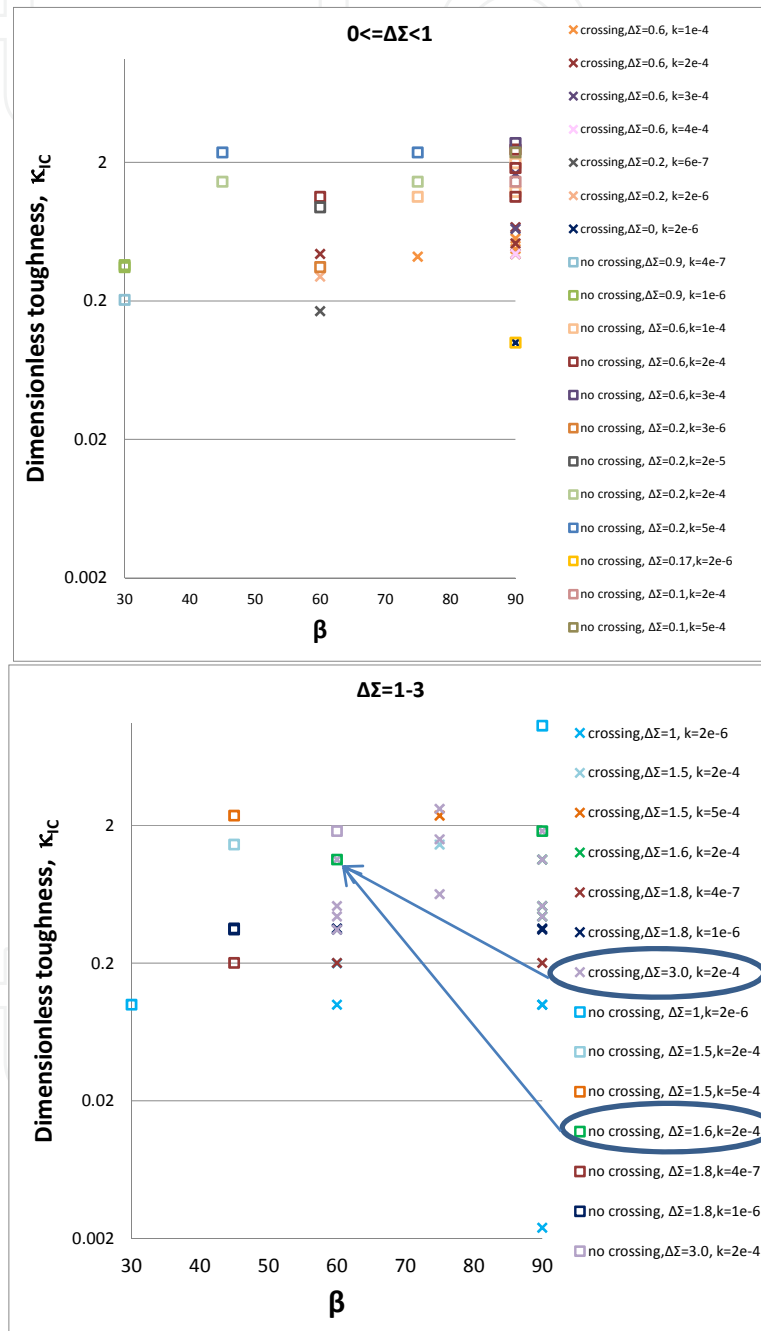

Figure 4. Crossing vs. arresting diagram in (κ_{IC}, β) for different range of relative stress contrast. $\kappa_{IC}^{(NF)} = 0$.
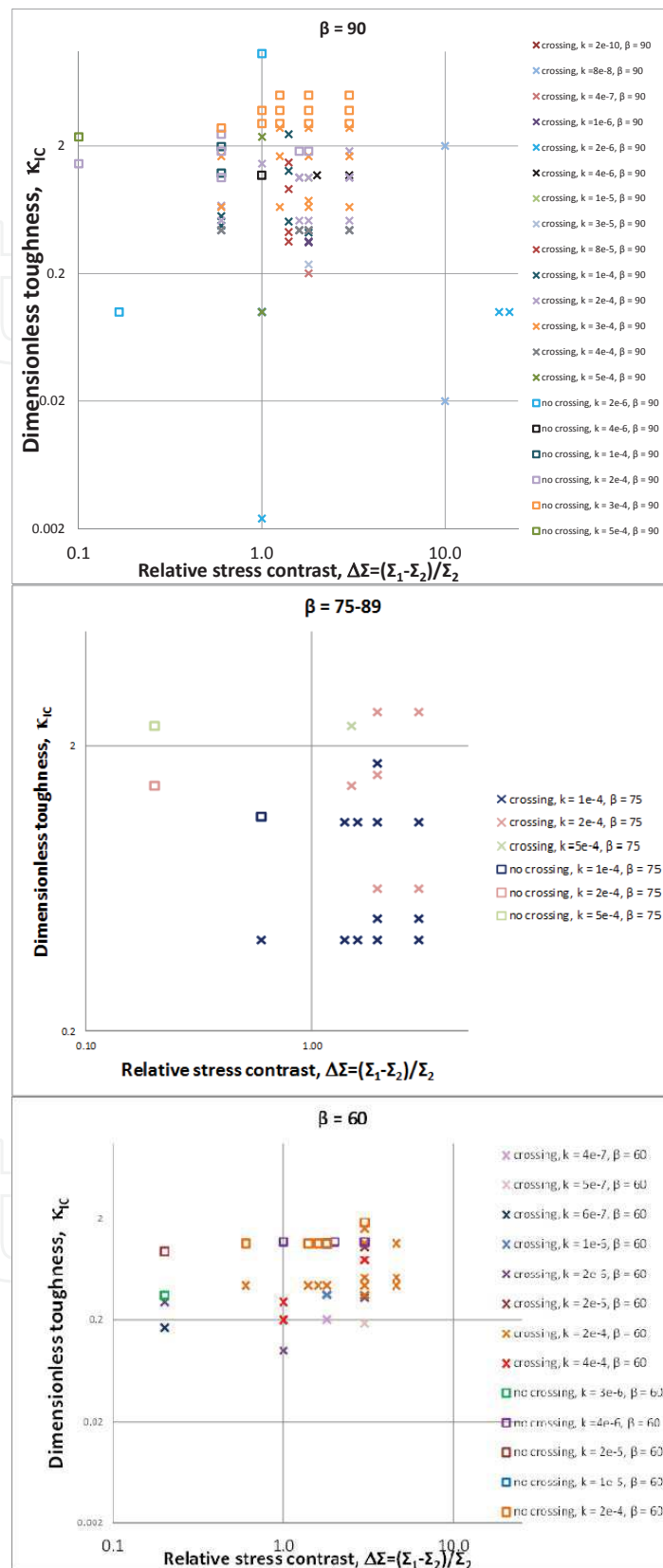
Figure 5. Crossing vs. arresting diagram in (κ_{IC}, $\Delta\Sigma$) for different angles of fracture interaction. $\kappa_{IC}^{(NF)} = 0$.
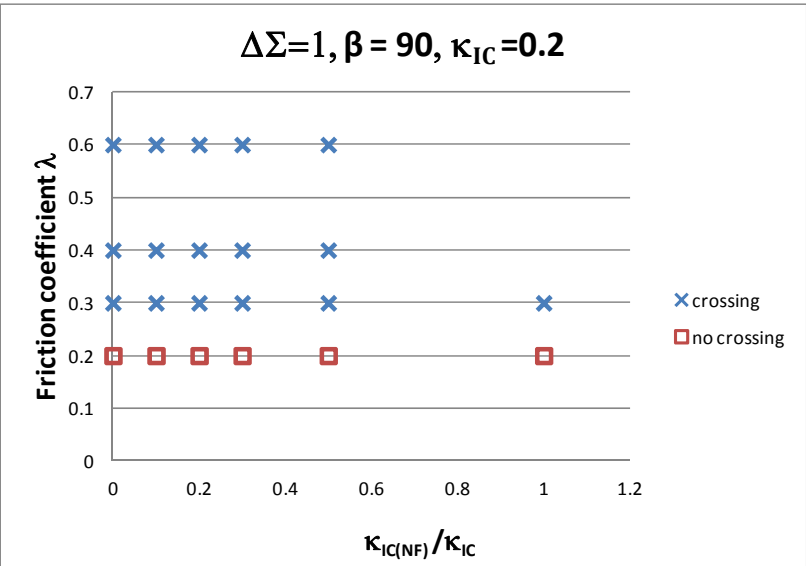
Figure 6. Crossing vs. arresting diagram in (λ, $\kappa_{IC(NF)}/\kappa_{IC}$).

5. Effect of NF permeability

5.1. Analytical model

The numerical investigation of the HF-NF interaction with the help of MineHF2D code did not allow us to extract the dependency of the fracture interaction outcome on the permeability of the NF. To accomplish the goal of the parametric study, we built an analytical model of the T-shape contact between the HF and the permeable NF with the following assumptions (Fig. 7).
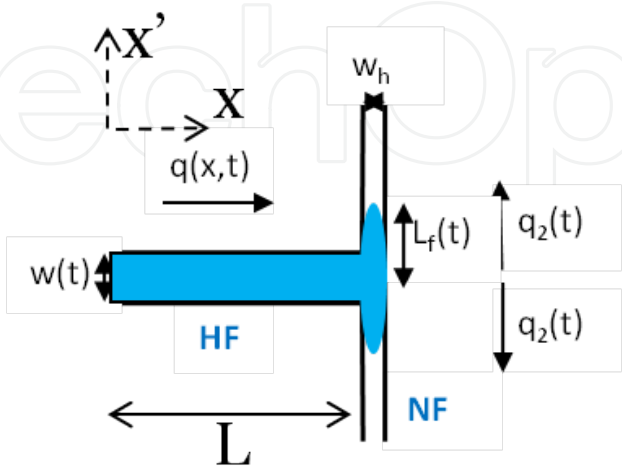

Figure 7. Illustration of the HF-NF interaction scheme in analytical model

Consider the HF in a T-shape contact with a permeable NF as schematically shown in Fig. 7. Both fractures have uniformly distributed but different hydraulic openings. After the contact, the fracturing fluid penetrates the NF from the tip of the HF. Representation of the HF with blunted tip of width w is realistic when the HF contacts a frictionally weak NF [25]. The NF remains mechanically closed with finite hydraulic conductivity described by the residual hydraulic opening w_h. It is assumed that w_h does change with time and the NF remains mechanically closed all the time. We also neglect fluid lag in the HF and solve the problem assuming that the injected fluid entirely fills the HF right after contact. The fracturing fluid penetrates the NF from the junction point symmetrically on both sides along the NF (Fig. 7).

First, we prescribe the uniform distribution of the fluid pressure along the HF from the inlet point to the contact point:

$$p_f(x,t) = p_0(t) \tag{24}$$

where p_0 is the fluid pressure at the inlet. The approximate solution of the elasticity equation for the opening of the HF w can be written as

$$w(t) = \frac{4L}{E'} [p_0(t) - \sigma_2] \tag{25}$$

where σ_2 is the minimum far-field stress.

Poiseuille's law and continuity equation for the fluid flow $q(x,t)$ along the HF are described by Eqns. (6–7). The fluid flow rate at the junction point is denoted as

$$q(x = L) = q^* \tag{26}$$

As long as $w = w_h = \text{const}$ along the NF, the Poiseuille's law and continuity equation can be written for the fluid flow along the NF as

$$\begin{cases} q_2 = -\dfrac{w_h^3}{12\mu} \dfrac{dp_{f2}}{dx'} \\ \dfrac{dq_2}{dx'} \end{cases} \tag{27}$$

where q_2 is the fluid flow rate along the NF on one side of the junction point (see Fig. 7), and $p_{f2}(x',t)$ is the distribution of fluid pressure in the NF. As the fluid penetrates the NF symmetrically from the junction point, using (26) we can write

$$q_2(t) = \frac{1}{2} q^*(t) \tag{28}$$

For steady flow the fluid pressure at the fracture junction point must be the same at the HF and NF sides, so using assumption (24) we write

$$p_{f2}(x' = 0) = p_f(x = L) \approx p_0(t) \tag{29}$$

The total fluid mass balance in the system of the HF and the NF can be written by making use of continuity equations (6) and (27), inlet condition (10), and elasticity equation (25) as follows:

$$Q = \frac{d}{dt}(\int_0^L w \, dx + 2 \int_0^{L_f} w_h \, dx') = \frac{4L^2}{E'} \frac{dp_0}{dt} + 2w_h \dot{L}_f \tag{30}$$

where L_f is the length of fluid penetration into the NF, and the upper point denotes the differentiation with respect to time. Using now the fluid flow equations (27) and the pressure relationship at the junction point (29), we can write

$$q_2 = w_h \dot{L}_f = \frac{w_h^3}{12\mu} \frac{p_0}{L_f} \tag{31}$$

Thus, from (30) and (31) we obtain the following system of ordinary differential equations for the fluid penetration length L_f and fluid pressure at the inlet p_0

$$\begin{cases} \dot{L}_f = \frac{w_h^2}{12\mu} \frac{p_0}{L_f} \\ Q - 2w_h \dot{L}_f = \frac{4L^2}{E'} \dot{p}_0 \end{cases} \tag{32}$$

The solution of these equations can be found after setting up the initial condition at the time of fracture contact, $t = 0$. We presume the fluid pressure at the HF tip is prescribed and there is not yet fracturing fluid penetration into the NF. The initial conditions are thus written as

$$\begin{cases} p_0(0) = p_{00} \\ L_f(0) = 0 \end{cases} \tag{33}$$

Rewriting the equations (32) and initial conditions (33) in terms of dimensionless parameters already introduced, and using substitutions $L_f = L \, \gamma_f$, $w_h = W \Psi_h$, $p_0 = P \Pi_0$, $t = T \tau$, we get

$$
\begin{cases}
\dot{\gamma}_f = \Psi_h^2 \dfrac{\Pi_0}{\gamma_f} \\[2mm]
1 - 2\Psi_h \dot{\gamma}_f = 4\dot{\Pi}_0 \\[2mm]
\gamma_f(0) = 0 \\[2mm]
\Pi_0(0) = \Pi_{00}
\end{cases}
\tag{34}
$$

Numerical solution of the problem (34) is plotted in Fig. 8. Fluid penetration length (Fig. 8, left) grows fast at the very beginning ($\tau \ll 1$) and turns to nearly linear dependence on time when $\tau > 1$. The pressure at the junction point drops right after the HF-NF contact (Fig. 8, right). The velocity of pressure drop rapidly slows, and after the certain inflection point it starts to grow linearly. As it will be shown later, the inflection point depends on the NF permeability and initial fluid pressure at fracture contact.

The numerical solution helps in the general solution of the problem (34) but hides the parametrical dependency of the fluid penetration and pressure behavior shown in Fig. 8. To evaluate the pressure inflection point τ^* and reveal the parametric sensitivity of the velocity of fluid penetration into the NF and the HF pressure dynamics during the contact, we further investigate the asymptotical behavior of the fluid length γ_f and the fluid pressure Π_0 at the very beginning of fracture contact and at large time after contact.
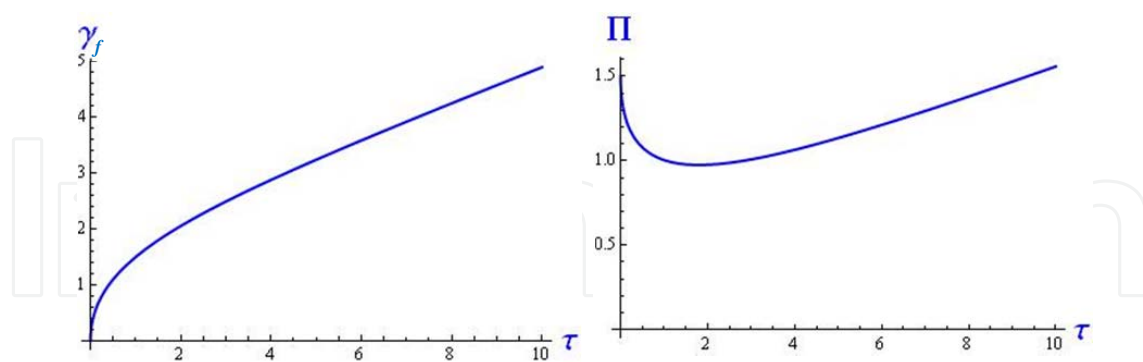

Figure 8. Analytical solution of the dimensionless problem for fluid penetration into NF (34) for dimensionless permeability $\Psi_h = 1$, and initial pressure $\Pi_{00} = 1.5$. Left plot is the dimensionless fluid front propagation along the NF in time. Right plot is the change of dimensionless pressure at the HF-NF intersection point.

Early-time (left) asymptote: $0 < \tau \ll \tau^*$.

Let us assume the following law for the fluid pressure and penetration length at the beginning of fracture contact,

$$\Pi_0 = \Pi_{00} - \Pi_1 \sqrt{\tau}$$
$$\gamma_f = v_f \sqrt{\tau} \tag{35}$$

where Π_1 and v_f are unknown positive constants that must be determined. After substitution of (35) in (34), in the limit $\tau \ll 1$ we arrive at the following relations for Π_1 and v_f:

$$\begin{cases} v_f^2 = 2\Psi_h^2 \Pi_{00} \\ 2\Pi_1 = \Psi_h v_f \end{cases} \tag{36}$$

The unknown constants Π_1 and v_f are thus found as

$$\begin{cases} \Pi_1 = \Psi_h^2 \sqrt{\Pi_{00} / 2} \\ v_f = \Psi_h \sqrt{2\Pi_{00}} \end{cases} \tag{37}$$

From this analysis it is obvious that the rate of fluid pressure drop at the beginning of fracture contact as well as the velocity of fluid penetration into the NF are affected more strongly by the permeability of the NF Ψ_h than by the initial fluid pressure in the HF Π_{00}.

The asymptotes (35) can be plotted with the accurate numerical solution of the equations (34). Fig. 9 shows the comparison of the numerical solution of the problem and asymptotes (35) with coefficients (37).
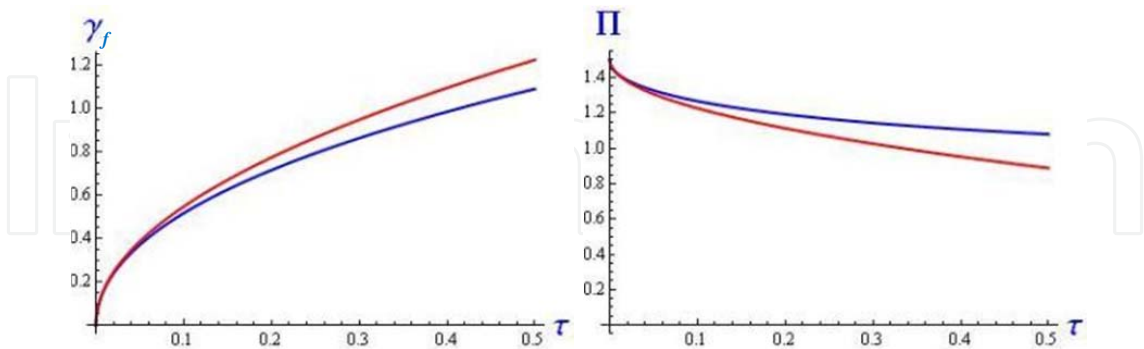

Figure 9. Asymptotic (red) and numerical (blue) solutions for the dimensionless fluid penetration length (left) and fluid pressure in junction point (right) at the early time of fracture contact

Large-time (right) asymptote: $\tau \gg \tau^*$

Now consider the large-time behavior of the system of contacted fractures. In that limit let us employ the linear asymptotes for the pressure and fluid penetration length

$$\Pi_0 = \Pi_1 \tau$$
$$\gamma_f = v_f \tau \tag{38}$$

where Π_1 and v_f are new unknown positive constants. From (34) we then obtain

$$\begin{cases} v_f^2 = \Psi_h^2 \, \Pi_1 \\ 1 - 2\Psi_h v_f = 4\Pi_1 \end{cases} \tag{39}$$

Solution of (39) for the unknown Π_1 and v_f gives the expressions

$$\begin{cases} \Pi_1 = \dfrac{1}{4} - \dfrac{\Psi_h^2}{8}\left[\sqrt{\Psi_h^4 + 4} - \Psi_h^2\right] \\ v_f = \dfrac{\Psi_h}{4}\left[\sqrt{\Psi_h^4 + 4} - \Psi_h^2\right] \end{cases} \tag{40}$$

Comparison of the asymptotes (38) with numerical solution of the equations (34) gives excellent agreement. Fig. 10 demonstrates this comparison.
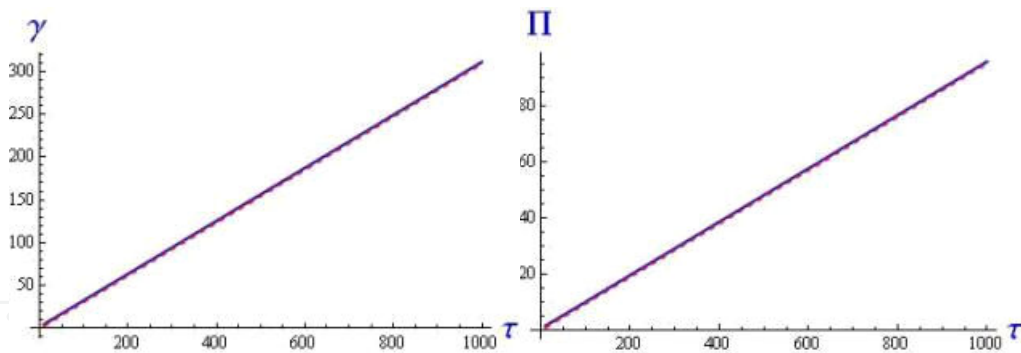

Figure 10. Asymptotic (red) and numerical (blue) solutions for the dimensionless fluid penetration length (left) and fluid pressure at junction point at large time of fracture contact

The inflection point: $\tau = \tau^*$, $\dot{\Pi}_0 = 0$

To find the parametric expression for the inflection point in time scale, where the fluid pressure starts to increase, we substitute $\dot{\Pi}_0 = 0$ into the second equation of (34) and have

$$\dot{\gamma}_f = \frac{1}{2\Psi_h} \tag{41}$$

If τ^* is close to zero, the velocity of fluid penetration can be taken from the early-time solution (35) with (37):

$$\dot{\gamma}_f = \Psi_h \sqrt{\frac{\Pi_{00}}{2\tau^*}} \tag{42}$$

Comparing now (41) with (42), one obtains the following estimation for the time of pressure drop-growth inflection:

$$\tau^* = 2\Pi_{00}\Psi_h^4 \tag{43}$$

This simple expression tells again that practically it is the magnitude of NF permeability that plays a key role in the transient pressure behavior and intensity of NF infiltration by the fracturing fluid.

5.2. Numerical simulations

To validate the analytical model predictions we performed several numerical simulations by MineHF2D code with κ_{IC}=0.32, Σ_2=0.8, $\Delta\Sigma$=1, β=90, λ=0.2 and various permeabilities of the NF. The residual hydraulic opening of the NF Ω_h in these numerical runs was intentionally chosen to be a magnitude close to the average opening of the HF at the point of intersection.

Fig. 11 shows the results of simulations for three different values of the residual hydraulic opening prescribed at the NF Ω_h : 1 mm, 0.1 mm, and 0.01 mm. In all these test cases the average opening of the HF close to the fracture intersection was 3 mm. Pressure records at the injection point and the length of fluid penetration into the NF after the fracture contact are compared with predictions of the analytical model and shown in Fig. 11 (left top and left bottom).

For two cases with lower NF permeability (green-, red-dashed line in Fig. 11) the pressure starts to grow immediately after the fracture intersection. As the fluid weakly propagates into the NF in these cases, the net pressure and HF opening almost equally quickly grow with time. In the second example, for Ω_h = 0.1 mm at t = 0.55 s, the NF opens mechanically as a result of increased net pressure of the penetrated fluid and the penetration rate increases (red line, Fig. 11); the pressure and opening of the HF decrease because of the enhanced leakoff along the NF.

In the third case, when the residual hydraulic opening at the NF is of the same order of magnitude as the average opening of the HF (3 times less), we observe comparably fast fluid leakoff into the NF after the contact (blue line, Fig. 11), which given the fixed injection rate into the HF does not allow the net pressure in the HF to grow. Very soon after the fluid reaches the tips of the NF prescribed in the numerical model (1.5 m in this example), the NF rapidly opens mechanically and the HF opening starts to grow.

Careful investigation of the complex dynamics of fluid-coupled fracture interaction deserves a separate work.
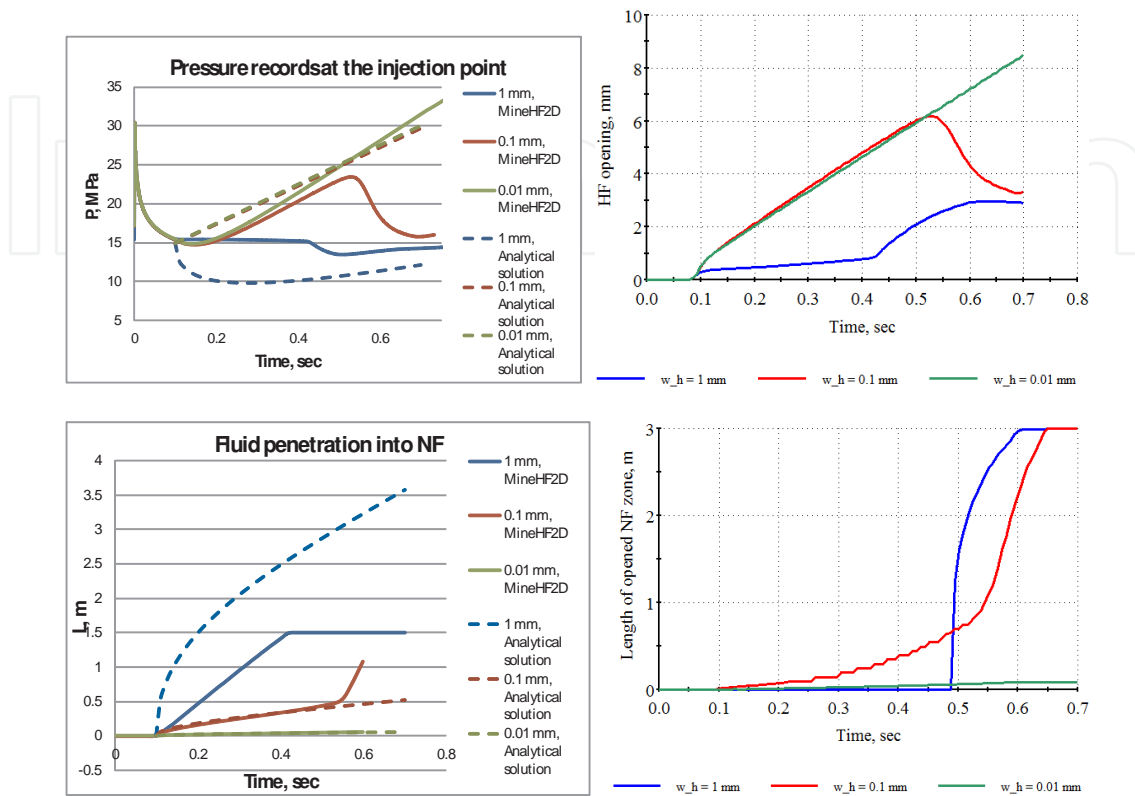

Figure 11. Results of numerical experiments with $\kappa_{IC} = 0.32$, $\Sigma_2 = 0.8$, $\Delta\Sigma = 1$, $\beta = 90$, $\lambda = 0.2$ and three values of residual hydraulic opening at the NF permeability (blue: 1 mm; red: 0.1 mm; green: 0.01 mm). Top left: fluid pressure changes at the inlet. Top right: opening of the HF at junction. Bottom left: fluid penetration length along the NF. Bottom right: total length of the mechanically open zone at the NF in meters.

6. Conclusions

In conclusion, we conducted an extensive parametric study of the problem of HF-NF interaction by means of numerical simulator MineHF2D developed by CSIRO. This research was mainly focused on the result of fracture interaction in terms of crossing or arresting of the HF at the NF as a function of the most sensitive parameters, such as fracture approach angle β, friction coefficient λ, dimensionless toughness κ_{IC}, inversely proportional to the injection rate and fluid viscosity, relative stress contrast $\Delta\Sigma$, and the NF permeability k.

In a system of interacting hydraulic and NFs, the number of physical parameters that can affect the result of interaction is large. The proper scaling of the problem allowed us to decrease the number of independent parameters from 14 dimensional parameters to 9 dimensionless parameters, and effectively perform the parametric study in the space of 6 of the most critical dimensionless parameters. We summarized the results of the large number of numerical

simulations performed in the range of parameters values relevant to fracturing field operations. The resultant solid picture of parametric sensitivity to the arresting versus crossing behavior helps provide a better understanding of the relative role of each parameter. In particular, aside from the well-known effect of the fracture approach angle and stress contrast, we revealed the influence of the injection rate and fluid viscosity on reducing the angle and stress threshold for HF-NF crossing.

The presented analytical model of the infiltration of the permeable NF by the contact with the HF allowed us to understand a parametric dependency of the HF pressure response and fracturing fluid penetration at early and large time after the HF-NF contact. We have seen a predominant role of the hydraulic permeability of the NF in the evaluation of the pressure decay curve after the fracture contact. It appears that at T-shape fracture contact, initially the pressure quickly drops and after some saturation it rebounds to grow. The rebound time of pressure response τ^* separating the early and large time regimes is strongly dependent on the permeability of the NF (as its forth power) and to a much lesser extent by fluid pressure at the HF-NF junction (linearly). Such fast pressure decay means that during $\tau < \tau^*$ the fluid penetration supports temporal arrest of the HF by the NF. Independent numerical computations with large residual aperture of the NF led us to the conclusion that the result of HF-NF interaction is affected by permeable properties of the NF only when the residual opening of the NF is comparable in magnitude with the opening of the HF at the contact.

Acknowledgements

Author details

Dimitry Chuprakov[1*], Olga Melchaeva[2,3] and Romain Prioul[1]

*Address all correspondence to: dchuprakov@slb.com

1 Schlumberger-Doll Research, Cambridge, MA, USA

2 Schlumberger-Doll Research, Cambridge, MA, USA

3 JSC Gazprom neft, Saint Petersburg, Russian Federation

References

[1] Valko P, Economides MJ. Hydraulic Fracture Mechanics: John Wiley & Sons; 1995.

[2] Fjær E, Holt RM, Horsrud P, Raaen AM, Risnes R. Petroleum related rock mechanics, Chapter 11 Mechanics of hydraulic fracturing. In: Fjaer E, Raaen AM, Risnes R, Holt RM, Horsrud P, editors. 2008. p. 369-390.

[3] Warpinski NR, Mayerhofer MJ, Vincent MC, Cipolla CL, Lolon EP. Stimulating Unconventional Reservoirs: Maximizing Network Growth While Optimizing Fracture Conductivity, SPE-114173-PA, 2009.

[4] Vincent M. Restimulation of Unconventional Reservoirs: When Are Refracs Beneficial? SPE-136757-PA, 2011.

[5] Vincent MC. Examining Our Assumptions—Have Oversimplifications Jeopardized Our Ability to Design Optimal Fracture Treatments? SPE Hydraulic Fracturing Technology Conference; The Woodlands, Texas, 2009.

[6] Thiercelin M. Hydraulic fracture propagation in discontinuous media. Presented at the International Conference on Rock Joints and Jointed Rock Masses, Tucson, Arizona, USA, 7-8 January. 2009.

[7] Cipolla CL, Warpinski NR, Mayerhofer MJ. Hydraulic Fracture Complexity: Diagnosis, Remediation, and Exploitation. SPE Asia Pacific Oil and Gas Conference and Exhibition; 01/01/2008; Perth, Australia: Society of Petroleum Engineers; 2008.

[8] Daneshy AA. Hydraulic Fracture Propagation in the Presence of Planes of Weakness. SPE European Spring Meeting; Amsterdam, Netherlands, 1974.

[9] Keer LM, Chen SH. Intersection of a Pressurized Crack with a Joint. Journal of Geophysical Research. 1981;86(B2):1032-8.

[10] Blanton TL. An Experimental Study of Interaction Between Hydraulically Induced and Pre-Existing Fractures. SPE Unconventional Gas Recovery Symposium; Pittsburgh, Pennsylvania, 1982.

[11] Cooke ML, Underwood CA. Fracture termination and step-over at bedding interfaces due to frictional slip and interface opening. J Struct Geol. 2001 Feb-Mar;23(2-3): 223-38.

[12] Zhang X, Jeffrey RG. The role of friction and secondary flaws on deflection and re-initiation of HFs at orthogonal pre-existing fractures. Geophys J Int. 2006 Sep;166(3): 1454-65.

[13] Zhang X, Jeffrey RG. Reinitiation or termination of fluid-driven fractures at frictional bedding interfaces. J Geophys Res-Sol Ea. 2008 Aug 28;113(B8)

[14] Zhang ZX, Kou SQ, Lindqvist PA, Yu Y. Relationship between fracture toughness and tensile strength of rock. Strength Theories: Applications, Development and Prospects for 21st Century. 1998:215-9.

[15] Gu H, Weng X, Lund JB, Mack MG, Ganguly U, Suarez-Rivera R. Hydraulic Fracture Crossing Natural Fracture at Non-Orthogonal Angles, A Criterion, Its Validation and Applications. SPE Hydraulic Fracturing Technology Conference; The Woodlands, Texas, 2011.

[16] Taleghani AD. Fracture Re-Initiation As a Possible Branching Mechanism During Hydraulic Fracturing. 44th US Rock Mechanics Symposium and 5th US-Canada Rock Mechanics Symposium; Salt Lake City, Utah: American Rock Mechanics Association; 2010.

[17] Blanton TL. Propagation of Hydraulically and Dynamically Induced Fractures in Naturally Fractured Reservoirs. SPE Unconventional Gas Technology Symposium; Louisville, Kentucky, 1986.

[18] Renshaw CE, Pollard DD. An Experimentally Verified Criterion for Propagation across Unbounded Frictional Interfaces in Brittle, Linear Elastic-Materials. International Journal of Rock Mechanics and Mining Sciences & Geomechanics Abstracts. 1995 Apr; 32(3):237-49.

[19] H.Gu, X.Weng. Criterion For Fractures Crossing Frictional Interfaces At Non-orthogonal Angles. 44th US Rock Mechanics Symposium and 5th US-Canada Rock Mechanics Symposium; Salt Lake City, Utah: American Rock Mechanics Association; 2010.

[20] Zhang X, Jeffrey RG, Thiercelin M. Mechanics of fluid-driven fracture growth in naturally fractured reservoirs with simple network geometries. Journal of Geophysical Research. 2009;114.

[21] Beugelsdijk LJL, Pater CJd, Sato K. Experimental Hydraulic Fracture Propagation in a Multi-Fractured Medium. SPE Asia Pacific Conference on Integrated Modelling for Asset Management; Yokohama, Japan, 2000.

[22] Pater CJd, Beugelsdijk LJL. Experiments and numerical simulation of hydraulic fracturing in naturally fractured rock. 25-29 June 2005: American Rock Mechanics Association; 2005.

[23] Wu R, Kresse O, Weng X, Cohen C-e, Gu H. Modeling of Interaction of Hydraulic Fractures in Complex Fracture Networks. SPE Hydraulic Fracturing Technology Conference; The Woodlands, Texas: Society of Petroleum Engineers; 2012.

[24] Zhang X, Thiercelin MJ, Jeffrey RG. Effects of Frictional Geological Discontinuities on Hydraulic Fracture Propagation. SPE Hydraulic Fracturing Technology Conference; College Station, Texas USA: Society of Petroleum Engineers; 2007.

[25] Warpinski NR, Teufel LW. Influence of Geologic Discontinuities on Hydraulic Fracture Propagation. SPE Journal of Petroleum Technology. 1987; 39(2).

[26] Chuprakov DA, Akulich AV, Siebrits E, Thiercelin M. Hydraulic-Fracture Propaga‐
tion in a Naturally Fractured Reservoir. SPE Production & Operations. 2011; 26(1).

[27] Chuprakov D, Melchaeva O, Prioul R. Injection-sensitive mechanics of HF interaction
with discontinuities. The 47th US Rock Mechanics Symposium (USRMS); San Fran‐
cisco, CA, 2013.

[28] Kresse O, Weng X, Chuprakov D, Prioul R. Effect of Flow Rate and Viscosity on
Complex Fracture Development in UFM model. The International Conference for Ef‐
fective and Sustainable Hydraulic Fracturing; 20-22 May 2013; Brisbane, Australia,
2013.

[29] Zhang X, Jeffrey RG, Thiercelin M. Deflection and propagation of fluid-driven frac‐
tures at frictional bedding interfaces: A numerical investigation. J Struct Geol. 2007;
29(3):396-410.

[30] Crouch SL, Starfield AM. Boundary Element Methods In Solid Mechanics: George
Allen & Unwin; 1983.

[31] Cheng AHD, Detournay E. On singular integral equations and fundamental solu‐
tions of poroelasticity. Int J Solids Struct. 1998 Dec;35(34-35):4521-55.

[32] Hills DA, Kelly PA, Dai DN, Korsunsky AM. Solution of crack problems. The distrib‐
uted dislocation technique. Solid Mechanics and its Applications. 1996;44.

[33] Leguillon D. Strength or toughness? A criterion for crack onset at a notch. Eur J Mech
a-Solid. 2002 Jan-Feb;21(1):61-72.

[34] Erdogan F, Sih GC. On the crack extension in plates under plane loading and trans‐
verse shear. Journal of Basic Engineering. 1963;85:519-27.

[35] Prioul R, Karpfinger F, Deenadayalu C, Suarez-Rivera R. Improving Fracture Initia‐
tion Predictions on Arbitrarily Oriented Wells in Anisotropic Shales. Canadian Un‐
conventional Resources Conference; 15-17 November 2011; Alberta, Canada: Society
of Petroleum Engineers; 2011.

[36] King GE. Thirty Years of Gas Shale Fracturing: What Have We Learned? SPE Annual
Technical Conference and Exhibition; Florence, Italy: Society of Petroleum Engineers;
2010.